Open access • Journal Article • DOI:10.1063/1.2357638

Structural, optical, and electrical properties of (Zn,Al)O films over a wide range of compositions — Source link

Jianguo Lu, Zhizhen Ye, Yu-Jia Zeng, Liping Zhu ...+4 more authors

Published on: 13 Oct 2006 - Journal of Applied Physics (American Institute of Physics)

Topics: Sputter deposition, Sputtering and Thin film

Structural, optical, and electrical properties of (Zn,Al)O films over a wide range of compositions

J. G. Lu,[a] Z. Z. Ye,[b] Y. J. Zeng, L. P. Zhu, L. Wang, J. Yuan, and B. H. Zhao
State Key Laboratory of Silicon Materials, Zhejiang University, Hangzhou 310027, People's Republic of China

Q. L. Liang
Quality Engineering Division, Semiconductor Manufacturing International Corp., Shanghai 201203, People's Republic of China

(Received 1 March 2006; accepted 31 July 2006; published online 13 October 2006)

(Zn,Al)O thin films have been prepared by a dc reactive magnetron sputtering system with the Al contents in a wide range of 0–50 at. %. The structural, optical, and electrical properties of (Zn,Al)O films were detailedly and systematically studied. The amount of Al in the film was nearly the same as, but often lower than, that in the sputtering target. The growth rate of films monotonically decreased as the Al content increased. In a low Al content region (<10 at. %), Al-doped ZnO (AZO) thin films could be obtained at 400 °C in an $Ar–O_2$ ambient with good properties. The optimal results of *n*-type AZO films were obtained at an Al content of 4 at. %, with low resistivity $\sim 10^{-4}$ Ω cm, high transmittance ~90% in the visible region, and acceptable crystal quality with a high *c*-axis orientation. The band gap could be widened to 3.52 eV at 4 at. % Al due to the Burstein-Moss shift [E. Burstein, Phys. Rev. **93**, 632 (1954)] modulated by many-body effects. An appropriate Al-doping concentration served effectively to release the residual, compressive stress in film, which may be the reason for the improvement in film stability and the increment in grain size as well. In a medium Al content region (10–30 at. %), however, the film quality was degraded, which was presumably due to the formation of clusters or precipitates in the grains and boundaries. Besides the (002) plane, other diffraction peaks such as (100) and (101) planes of ZnO were observed, but the (Zn,Al)O films still exhibited a single-phase wurtzite ZnO structure. An intragrain cluster scattering mechanism was proposed to interpret the reduction of carrier mobility in films with the Al contents in the 7–20 at. % region. The solubility limit of Al in ZnO film was identified to be in the 20–30 at. % range, much higher than the thermodynamic solubility limit of 2–3 at. % in ZnO. In a high Al content region (≥30 at. %), there were distinct observations for (Zn,Al)O films. As the Al content was 30 at. %, the film appeared in a two-phase nature with ZnO hexagonal and Al_2O_3 rhombohedral structures. At the 50 at. % Al content, the matrix of the (Zn,Al)O film was Al_2O_3, and no evident trace of wurtzite ZnO was observed. The electrical and optical properties for both cases were also very different from those at the Al contents below 30 at. %. © *2006 American Institute of Physics*. [DOI: 10.1063/1.2357638]

I. INTRODUCTION

Zinc oxide (ZnO) is a II-VI compound semiconductor with a wide direct band gap of 3.37 eV and a large exciton binding energy of 60 meV at room temperature.[1–3] The band gap of ZnO can be tuned by alloying with Cd or Mg; the resultant (Zn,Cd)O and (Zn,Mg)O alloys have allowed gap energies covering the range of 2.8–4.5 eV in practice.[4–7] Besides these contributions, ZnO has other advantages, including the following: (1) abundant raw materials and hence low cost in production, (2) environmental friendliness, (3) high radiation resistance, (4) low thermal budget required for thin-film deposition, and (5) commercial availability of large-area single-crystal ZnO substrates.

Nominally pure ZnO is a *n*-type semiconductor, but its optical and electrical properties seem to be not very stable, especially at high temperatures.[8,9] For practical purposes, doped *n*-type ZnO is usually preferred. The low-resistivity *n*-type ZnO could be realized by doping with group IIIA [e.g., B,[10,11] Al,[12–31] Ga,[32–34] and In (Refs. 35 and 36)], IIIB [e.g., Sc (Ref. 37) and Y (Ref. 37)], IV [e.g., Si,[38] Ge,[39] and Sn (Ref. 40)], and VII [e.g., F (Ref. 41) and Cl (Ref. 42)] elements. Among these possible dopants, Al is the best one, popularly used in growth process resulting in high-quality, low-resistivity Al-doped ZnO (AZO) thin films.[12–31] AZO is a key functional oxide that exhibits strong ultraviolet emission, high transparence to visible light, and high conductivity. As a transparent conducting oxide (TCO), AZO is regarded as an ideal candidate for replacing tin-doped indium oxide (ITO) and tin oxide (NESA) commercially used nowadays,[43–46] owing to its desired properties mentioned above as well as its nontoxicity, long-term environmental stability, and easier etchability. In addition, the recent success in creating *p*-type conductivity in ZnO makes it very promising for use in ultraviolet (UV) and blue optoelectronic devices such as light-emitting diodes (LEDs) and laser di-

[a]Electronic mail: lujianguo@zju.edu.cn
[b]Electronic mail: yezz@cmsce.zju.cn

odes (LDs).[47–50] AZO thin films are considered naturally as an ideal *n*-type layer for the heterostructure device design.[51–53]

AZO thin films could be prepared by various techniques, such as thermal evaporation,[12] magnetron sputtering,[13–23] chemical vapor deposition (CVD),[24] pulsed laser deposition (PLD),[25–27] molecular beam epitaxy (MBE),[28] sol gel,[29] and spray pyrolysis.[30,31] Regardless of the preparation method, however, almost all studies have been focused just on the low Al content region, commonly lower than 7 at. %.[12–31] This Al content region may be ideal for achievement of good *n*-type ZnO. As we already know, Al plays a crucial role in determining the properties of AZO films. In this regard, this narrow range limited in studies may prevent us from fully understanding the Al-doping mechanism in ZnO. In fact, we have had no complete knowledge of the Al-doped ZnO films so far, with a number of confusing issues including the solubility limitation of Al in ZnO, stability mechanism of AZO films, and scattering mechanism of carriers. For this purpose, we demonstrate a comprehensive study of Al-doped ZnO thin films in this work. The Al content is in a wide range of 0–50 at. %. To distinguish from the abbreviation of AZO usually used for Al-doped ZnO in the low Al content region, we adopt the symbol of (Zn,Al)O to express the Zn–Al–O system in the wide 0–50 at. % Al content region. The structural, electrical, and optical properties of (Zn,Al)O thin films are systematically discussed in this work.

This study is expected to provide further insight on the (Zn,Al)O film, and also to shed some light into the emergence of other issues in progress. For example, Al metal was commonly used as the electrode on a *n*-type ZnO layer to form an Ohmic contact.[54,55] A Au/*n*-ZnO Schottky barrier diode has been reported by depositing a ZnO film on an Al metal layer as the bottom electrode on a silicon substrate.[56] An alloying process would unavoidably occur at the metal-semiconductor (*M-S*) interface, where a high Al content might be involved. In addition, $ZnAl_2O_4$ is another attractive semiconductor in recent literatures, which was prepared commonly by a sintering process.[57,58] Gorla *et al.*[59] reported the formation of $ZnAl_2O_4$ by a solid-state reaction between the epitaxial ZnO film and Al_2O_3 substrate. This study could be expected to provide some useful information on these issues.

II. EXPERIMENT

Among various deposition methods, sputtering is the most widely used technique for preparing AZO films.[13–23] Accordingly, we have prepared (Zn,Al)O thin films by a dc reactive magnetron sputtering system. A series of disks of Zn–Al alloy metal (99.99% purity for both Zn and Al) with different Al contents (0, 1, 4, 7, 10, 15, 20, 30, and 50 at. %) was used as the target. Fused quartz and *n*-type Si (111) wafers were used as the substrates. Quartz wafers were degreased in an acetone ultrasonic bath, while Si wafers were cleaned by a typical RCA cleaning process; they were blow dried by N_2 gas for film deposition. The vacuum chamber was evacuated to a base pressure of 10^{-3} Pa with rotary and oil diffusion pumps, and then the sputtering gas mixture, O_2 and Ar (99.99% purity for both cases), was introduced directly into the dark space shields of the magnetrons. The partial pressures of O_2 and Ar were regulated by mass flow controllers and adjusted at a 30%-to-70% ratio before the ignition of the discharge. Prior to deposition of a film, the target was presputtered for 15 min with a shutter coving the substrate in order to remove any contaminant on the surface of the target and ensure stable sputtering conditions as well. The shutter was subsequently removed to commence growth. During the film deposition, the total working pressure was maintained at 5 Pa, and the substrate temperature was kept at 400 °C by a thermocouple positioned on the reverse side of the substrate holder. All the (Zn,Al)O films were deposited for 30 min and naturally cooled down to room temperature for property measurements. Two half wafers, one for quartz and another for Si, were symmetrically juxtaposed on the substrate holder for film deposition in any one growth to avoid the influence of any variation in sputtering parameters during different runs.

The crystal quality of (Zn,Al)O films was analyzed by x-ray diffraction (XRD) in θ-2θ geometry using a Bede D1 system. A Ni-filtered Cu $K\alpha$ source ($\lambda = 0.154\,06$ nm) was used, and the scanning range was between $2\theta = 20$ and 60°. The surface morphology of the films was evaluated by an FEI Sirion 200 FEG field-emission scanning electron microscope (FE-SEM). The film thickness was measured using a surface profiler (α-step 500, Tencor) and was confirmed using the interference fringes from optical transmission spectra. The chemical composition and Al concentration in the films were investigated by an energy dispersive x-ray (EDX) spectroscopy attached to the SEM. The electrical properties were carried out on an HL5500PC system of Bio-Rad Microscience using a four-point probe van der Pauw configuration and a spreading resistance technique (SSM-350) at room temperature. The optical transmission through film was performed with a Cary 100 ultraviolet-visible (UV-Vis) dual-beam spectrophotometer from 300 to 600 nm.

III. RESULTS AND DISCUSSIONS

A. Growth rate

We start by investigating how the growth rate is related to the Al content in the target. The growth rate was determined by dividing the film thickness by the sputtering time. This deposition parameter is important in film thickness control, particularly for precise multilayer preparation. Figure 1 shows the growth rate as a function of Al content in sputtering targets. The growth rate is 13.4 nm/min for the nominally pure ZnO film. The dc sputtering system generally has a high deposition rate, which is one of its merits.[13] The growth rate gradually decreases with the increase in Al content. This decreasing rate is slow in a low Al content region (<10 at. %), ranging from 12 to 13 nm/min, but it becomes evident in a medium Al content region (10–30 at. %), down from 11.6 nm/min at 10 at.% Al rapidly to 6.5 nm/min at 20 at. % Al. When the Al content is high (≥30 at. %), the decreasing rate becomes slow again, e.g., at 2.8 nm/min at 30 at. % Al and 1.4 nm/min at 50 at. % Al. The growth rate seems to saturate in a rather high Al content region. This

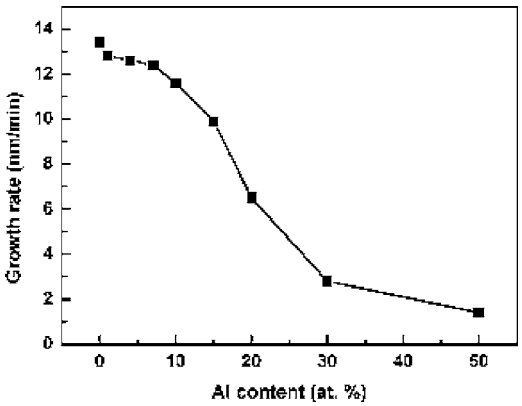

FIG. 1. Growth rate of (Zn,Al)O films as a function of the Al content in targets.

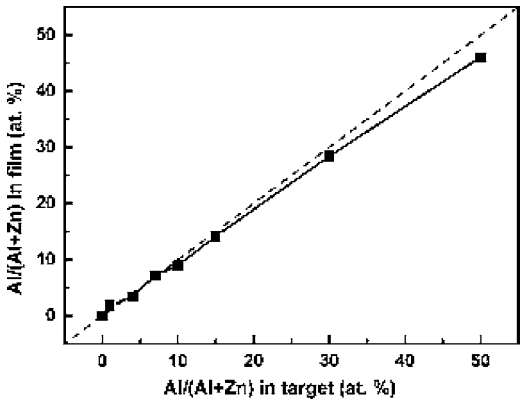

FIG. 3. Correlation between the Al content in (Zn,Al)O films and that in sputtering targets.

variation in growth rate is an indication that Al plays an important role in the (Zn,Al)O film deposition. The amount of atoms arriving at the substrate surface is expected to be inversely proportional to the Al content in the target. This decreasing arriving possibility could be explained by the decreasing sputtered atoms, since the sputtering becomes difficult with the Al content due to the lower sputtering yield of Al atoms and the target poisoning owing to the ease in forming an Al_2O_3 layer on the surface of the target.[13,14]

B. Film composition

The chemical composition of (Zn,Al)O films was analyzed by an EDX spectroscopy. The detection limit of quantitative analysis is ~0.5 at. % for EDX, which is applicable to our cases. Figure 2 shows the typical EDX spectrum corresponding to the (Zn,Al)O film prepared using a Zn–Al alloy target with an Al content of 4 at. %. In the EDX spectrum, peaks at 0.518, 1.109, 8.635, and 9.577 keV correspond to O $K\alpha$, Zn $L\alpha$, Zn $K\alpha$, and Zn $K\beta$, respectively. The peak at 1.496 keV is related to Al $K\alpha$. The atomic percentage (C_A) of the element in the matrix is given by

$$C_A = \frac{S_A I_A}{\sum_i S_i I_i}, \tag{1}$$

where S_A and I_A are the EDX sensitivity factor and integral count of element A, respectively. For the (Zn,Al)O film, $i=3$ is the number of elements presented including Zn, O, and Al. The calculated Al content in the film is 3.5 at. %, which is consistent with that in the target. Figure 3 shows the correlation of the Al content between the film and the target. The amount of Al in the film is nearly the same as, but often lower than, that in the sputtering target, with a relatively obvious derivation towards low values in the high Al content region. In previous literatures, Igasaki and Saito[15] and Kim *et al.*[16] pointed out that the amount of Al in the AZO film is almost independent of the deposition parameters including the Al content in targets. It seems to be plausible in the low Al content region owing to its less effect, but it is noted that the amount of Al in the resulting film, in fact, is correlated to that in the target. As can be seen in Fig. 3, the amount of Al in the (Zn,Al)O film is about 46.1 at. % when the Al content is 50 at. % in the target. This deviation is somewhat evident as a matter of fact. The phenomenon can also be attributed to the fact that the possibility of Al atoms arriving at the substrate surface is smaller than that of Zn atoms, as mentioned above. Here, we would like to emphasize that, for convenience, the Al content is always referred to as that in the target in this work, unless otherwise noted.

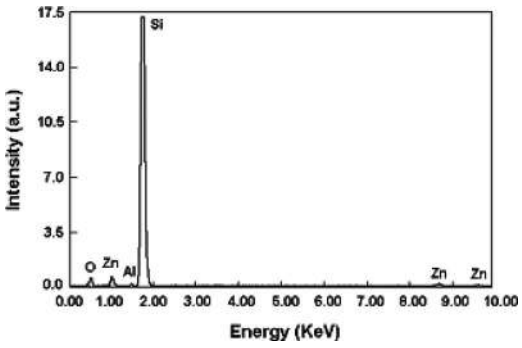

FIG. 2. EDX spectrum of the (Zn,Al)O film prepared with a 4 at. % Al content showing its chemical composition.

C. XRD analysis

The crystal structures of (Zn,Al)O films were investigated by XRD. The normalized XRD profiles were displayed in Figs. 4(a) and 4(b) for convenient illustrations. When the Al content ranges from 0 to 10 at. %, only one peak corresponding to the (002) plane of ZnO (Ref. 82) appears, and no other diffraction is observed, suggesting that these films are of a high c-axis preferential orientation. As the Al content is more than 10 at. % (e.g., at 15 at. %), besides the (002) peak, a small diffraction intensity from the (100) plane occurs. For the film with a 20 at. % Al content, the diffraction trace of the (002) plane is evidently weakened, while that of the (100) plane is enhanced, with an additional (101) diffraction peak observed in the XRD profile. The c-axis preferential orientation of the film becomes indistinct by the increase in doping concentration, suggesting the degradation of the film crystallinity. But it is noted that no diffraction peak from other phase is detected, so the (Zn,Al)O film is still of a single-phase wurtzite ZnO structure as the Al content is up to 20 at. %. With further increase of the Al content to 30 at. %,

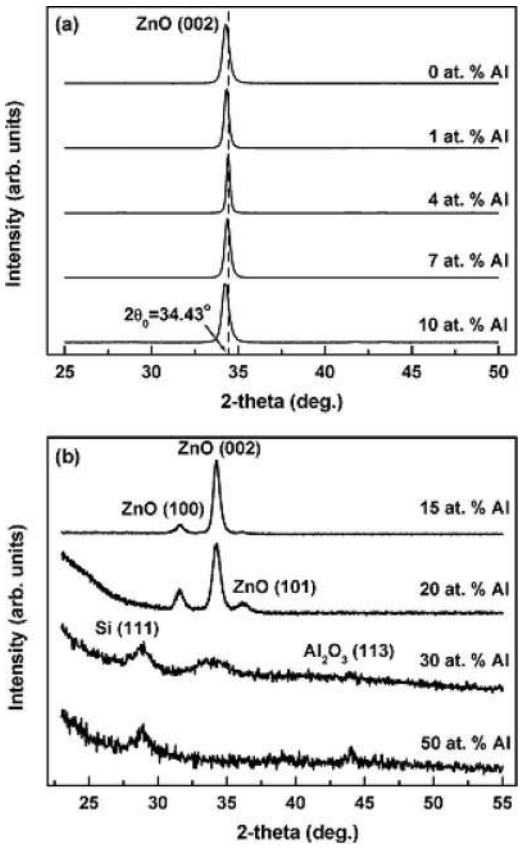

FIG. 4. XRD profiles of (Zn,Al)O films prepared with the Al contents of 0, 1, 4, 7, 10, 15, 20, 30, and 50 at. %. They are shown in (a) and (b) for convenient illustrations.

the ZnO (002) diffraction peak becomes very weak. A new diffraction peak located at $2\theta \sim 44.0°$ is observed, which corresponds to the (113) plane of α-Al_2O_3,[83] although its intensity is much smaller in the XRD pattern. The Si (111) peak which appeared in the XRD profile comes from the substrate. This is indicative of the appearance of the second phase. The (Zn,Al)O film is a two-phase mixture consisting of ZnO hexagonal and Al_2O_3 rhombohedral structures. Therefore, it is reasonable to conclude that the solubility limit of Al in the ZnO film is in the 20–30 at. % range. The thermodynamic solubility limit of Al in ZnO has been reported to be in the 2–3 at. % range,[60] much lower than that obtained in ZnO films here. Magnetron sputtering is a suitable growth method for providing a nonequilibrium state in the crystal deposition process, which enables us to fabricate solid solution films well above the thermodynamic solubility limit. At a very high Al content of 50 at. %, the diffraction trace of the ZnO (002) plane disappears, while the intensity of the Al_2O_3 (113) peak is strengthened evidently. It seems reasonable to consider that the matrix is Al_2O_3 rather than ZnO; that is to say, the (Zn,Al)O film, strictly speaking, is Zn-doped Al_2O_3 rather than Al-doped ZnO. It should be noted that, albeit the ZnO and Al_2O_3 diffraction peaks are observed at the 30 and 50 at. % Al contents, they are either in the steamed-bun shape or very weak. This is an indication that both samples are poor in film crystallinity or that they are noncrystalline, as a matter of fact. For all the (Zn,Al)O films, no $ZnAl_2O_4$ phase is detected. Semiconductor $ZnAl_2O_4$ powders have been fabricated usually by a sintering process.[57,58] There are few reports of preparing this material by a conventional semiconductor film deposition technique. The magnetron sputtering system may not be suitable for growth of $ZnAl_2O_4$ films.

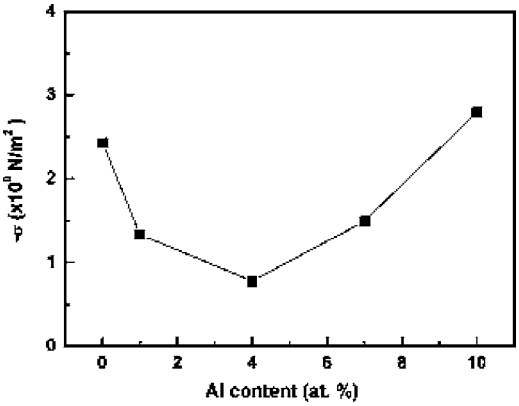

FIG. 5. Variation of the in-plane compressive stress in film with respect to the Al content ranging from 0 to 10 at. %.

As discussed above, the film quality is obviously degraded as the Al content is above 10 at. %. Thus, we are mainly concerned about the (Zn,Al)O or AZO films in the 0–10 at. % Al content region to clarify their characteristics. As displayed in Fig. 4(a), one of the significant observations in the XRD profiles is that the position of the (002) diffraction peak shifts to lower angles as compared with standard data ($2\theta_0 = 34.43°$) of the (002) peak, which manifests itself by the elongation of the *c*-axis lattice constant; that is to say, there is a residual stress in the plane of the films as compared with unstressed powder. For hexagonal crystals with a highly *c*-axis preferred orientation, this in-plane stress (σ) can be calculated based on the biaxial strain model,[61]

$$\sigma = [2C_{13} - C_{33}(C_{11} + C_{12})/C_{13}](c - c_0)/c_0. \quad (2)$$

Here, c is the lattice constant obtained from the (002) reflection in the XRD profile, c_0 is the corresponding bulk value (0.5206 nm), and C_{ij} are elastic stiffness constants ($C_{11} = 2.1 \times 10^{11}$ N/m^2, $C_{33} = 2.1 \times 10^{11}$ N/m^2, $C_{12} = 1.2 \times 10^{11}$ N/m^2, and $C_{13} = 1.05 \times 10^{11}$ N/m^2). This yields the following numerical relation for the stress derived from XRD:

$$\sigma = -4.5 \times 10^{11}(c - c_0)/c_0 \ (\mathrm{N/m^2}). \quad (3)$$

The calculated results are shown in Fig. 5. The negative sign indicates that the AZO films are in a state of compressive stress. The total stress in the film commonly consists of two components. One is the intrinsic stress introduced by impurities and defects in the crystal, and the other is the extrinsic stress introduced by the lattice mismatch and thermal expansion coefficient mismatch between the film and substrate. The latter component can be negligible compared to the stress measured,[17,62,63] and, moreover, it could be easily ruled out based on the obtained results since it should be independent of the Al content in AZO films. The former component is the main reason, as similarly believed in some other literatures,[9,62,64,65] which has the ability to identify the film structure. In addition, it is noted that there are several reports

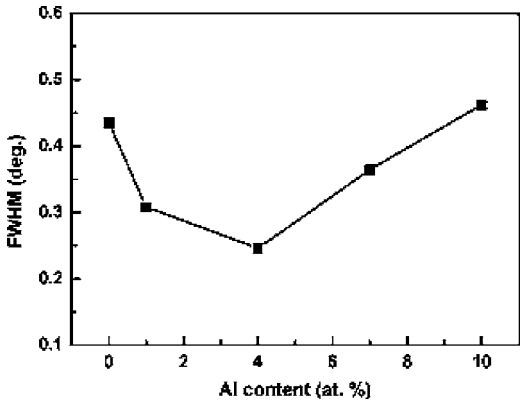

FIG. 6. Variation of FWHM in the (002) direction of (Zn,Al)O films with respect to the Al content in the range of 0–10 at. %.

that attribute the compressive stress in film to the energetic bombardment because of atomic peening in the sputtering process.[17,61] This effect, however, could also be readily ruled out based on our results. The energy per sputtered Zn or Al atom had no difference in any one growth since the growth conditions were exactly the same, except the gradually increasing Al-to-Zn ratios. The bombardment is an energy-dependent process, so the existing stress in film, if predominated by the bombardment-induced stress, should change monotonically, which is in contradiction with our experimental observation.

The undoped ZnO film is intrinsically *n* type with a compressive stress of about 2.43×10^9 N/m^2, suggesting that Zn interstitials may be predominant in nonstoichiometric pure ZnO.[62] When Al is incorporated into ZnO, the compressive stress decreases to 1.34×10^9 N/m^2 at 1 at. % Al; that is to say, the *c*-axis lattice constant becomes small. The ionic radii of Zn^{2+} and Al^{3+} are 0.06 and 0.039 nm, respectively, so the addition of Al to ZnO is expected to shorten the *c*-axis length if Al atoms are substituted into Zn sites in the crystal, having an effect on releasing the residually compressive stress in the as-deposited film. This effect seems to be comparable to observations, indicating that most Al atoms in the AZO films are substituted in Zn sites. It is reasonable to conclude that there is a certain critical concentration, which seems to be 4 at. % within our study. At this Al-doping concentration, the AZO film has a lowest compressive stress of 0.78×10^9 N/m^2. When the Al incorporation is above this critical concentration, excess Al atoms are located at interstitial sites, leading to the expansion of the hexagonal lattice and thus inducing the enhanced compressive stress in film. For example, the stress increases to 2.79×10^9 N/m^2 at 10 at. % Al. The substitutions and interstitials of Al atoms are the two competitive factors. Precise control of Al-doping concentration should be deliberately considered for engineering a nearly stress-free environment in AZO films. Since the stress is a strong driving force for instabilities, the relatively low stress in AZO films is expected to induce their stable behaviors and so improve the film quality.

Figure 6 shows the full width at half maximum (FWHM) of the (002) diffraction peak as a function of the Al content. The FWHM was corrected for instrumental broadening using the monocrystalline silicon (111) diffraction line. As the Al content increases from 0 to 10 at. %, the FWHM first decreases and then increases, reaching the smallest value of 0.25° at 4 at. %. The FWHM value is influenced by many factors such as grain size, stress distribution, and crystal imperfection. Regardless of the influencing factor, the FWHM value is widely used as a negative indicator of film quality. From this point of view, we could also draw the conclusion that the optimal Al content is 4 at. %, since the corresponding AZO film has the best crystal quality considering its smallest FWHM value.

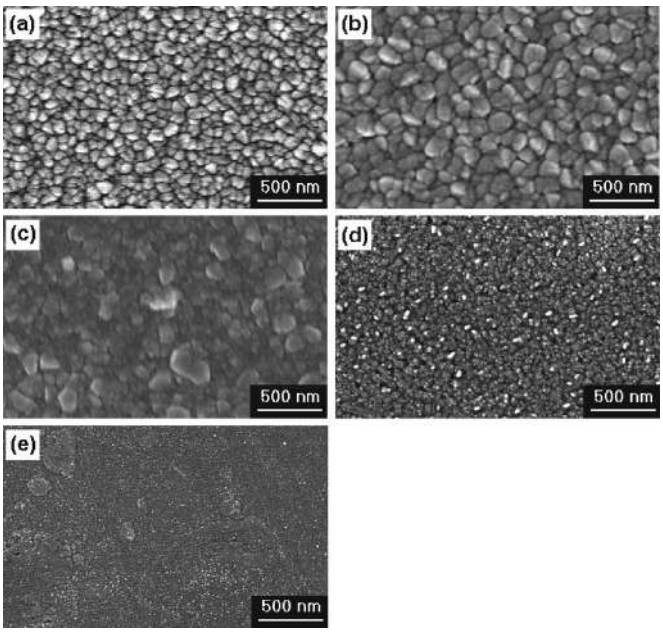

FIG. 7. SEM images of the (Zn,Al)O films prepared at different Al contents: (a) 0 at. %, (b) 4 at. %, (c) 15 at. %, (d) 30 at. %, and (e) 50 at. %.

D. SEM illustration

The morphologies of (Zn,Al)O were evaluated by the SEM micrographs. Figure 7 selectively displays the surface SEM images of samples prepared with Al contents of 0, 4, 15, 30, and 50 at. %. The undoped ZnO film consists of closed-packed and hexagonally shaped microcrystallines, arrayed regularly on the substrate with a narrow distribution of grain sizes. The AZO film with a 4 at. % Al content shows similar observations to the undoped ZnO film, except the evidently bigger grains with a more uniform grain distribution. For all the films in the 0–10 at. % Al content range, they have a smooth surface, and no visible voids and defects over the film are observed. As the Al content is up to 15 at. %, however, the surface is bumpy and rough, although the grain shape is still hexagonal faceted. The grains diminish evidently, and their distribution is inhomogeneous. Some big grains, accompanied with lots of pores, are observed clearly. This degradation in crystal quality displayed by SEM coincides with that by XRD, which is believed to be the result of the large amounts of defects and segregations caused by the high incorporation of Al in film. When the Al content increases to 30 at. %, an apparent transition is observed. The grain size is quite small, with an obscure grain shape. The (Zn,Al)O film is composed of two phases of ZnO

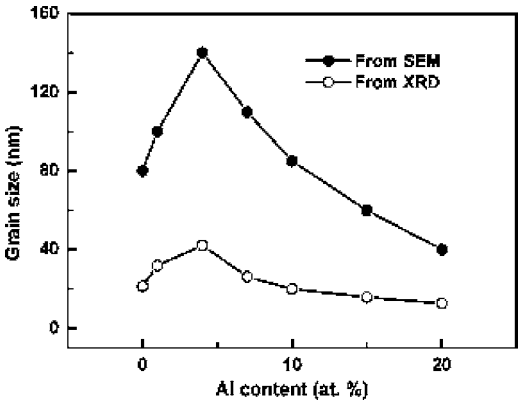

FIG. 8. Average grain sizes derived from SEM and XRD observations for (Zn,Al)O films prepared in the 0–20 at. % Al content range.

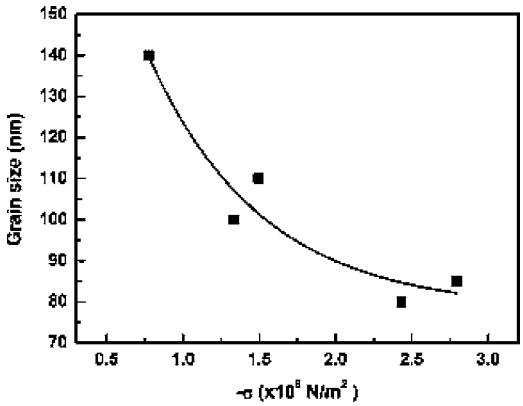

FIG. 9. Dependence of the grain size of (Zn,Al)O films on the in-plane compressive stress in films with the Al content ranging from 0 to 10 at. %.

and Al_2O_3, as confirmed by XRD. The phase separation could be readily identified from the corresponding SEM image. At the Al content of 50 at. %, the matrix of the resultant (Zn,Al)O film is Al_2O_3, as confirmed by XRD. The corresponding SEM image is shown in Fig. 7(e). The grain size is very small. Detailed investigations on (Zn,Al)O films in the high Al content range are now in progress.

Figure 8 shows the average grain sizes estimated from the SEM images for the (Zn,Al)O films with the Al content in the 0–20 at.% range. The grain size (d) can also be derived from XRD using the Debye-Scherer formula,

$$d = K\lambda/(\beta \cos \theta), \tag{4}$$

where K is the correction factor (0.89), λ is the x-ray wavelength (0.154 06 nm), β is the θ-2θ peak width (corrected for instrumental broadening), and θ is the Bragg diffraction angle. This formula is not limited by the preferential orientation and is valid for an ordinary XRD profile. We choose the (002) line to calculate the grain size since it is prominent in all the involved profiles. The calculated values are also shown in Fig. 8. The grain size obtained from SEM is larger by about a factor of 4 as compared with that determined from XRD. This difference is mainly caused by the different grain size criteria, underlying the different methods. The SEM grain sizes are measured by the distances between the visible grain boundaries, whereas the XRD method determines the extension of the crystalline that diffracts the x rays coherently, which is a more stringent criteria, thus leading to smaller grain sizes. However, in the entire compositional range studied the similar variation trend in grain size, regardless of the determining method, is obviously confirmed. For a unified illustration, the grain size mentioned below refers to that estimated from SEM. The average grain size is approximately 80 nm for the undoped ZnO film. As the Al content increases, the grain size first increases, reaching the largest value of 140 nm at 4.0 at. % Al, and then begins to decrease, down to about 40 nm at 20 at. % Al.

In general, the grain becomes small with the addition of impurities to the matrix material due to the induced defects and imperfection that behave as the source for forming grain boundaries.[18,30] In this regard, this observed change in grain size cannot be explained just by the conventional impurity effect. The increment in grain size with the addition of Al to ZnO, together with the improved film crystallinity, was once reported by Cebulla *et al.*[17] and Mass *et al.*[25] They attributed this observation to the beneficial role of Al as a surfactant in the growth process. As we know, the introduction of surfactants is an effective approach to facilitate the layer-by-layer (Frank–Van der Merwe) growth by modifying the growth mode, commonly used in the multilayer film preparation.[66–69] For a surfactant to function, it must fulfill two criteria:[68] it must be sufficiently mobile to avoid incorporation at a given growth rate, and it must surface segregate with the ability to lower the surface free energies of both layers. From this point of view, the surfactant role should be ruled out in principle in interpreting the effect of Al in ZnO films. Here, we propose a stress model to explain the observations in our work and other literatures as well. For obvious clarification, we plot the correlation between the grain size and compressive stress of the AZO films in Fig. 9. As the stress decreases, the size increases. This is an indication that the grain size (d) is directly related to the stress (σ) in the film. The exponential fitting gives the following experiential formula:

$$d = 78 + 175 \exp(1.35\sigma). \tag{5}$$

Here, d and σ are in units of nanometers and N/m^2, respectively. Also, σ is negative. Note that this formula is only valid for AZO films at the Al content less than 10 at. %. As discussed above, an optimum Al concentration could effectively serve to release the residual stress in films. Besides the attribute related to stabilities mentioned above, this stress reduction possibly plays additional twofold roles: (1) it diminishes the density of stress-induced defects (e.g., dislocations) in films, and so improves the crystal perfection, and (2) it behaves as a mechanism, replacing the formation of islands,[69] to relieve the strained system, and thus facilitates the two-dimensional (2D) growth. Both of the two roles have the beneficial effect on the grain growth. This effect of Al in ZnO films could therefore be named as the stress-release mechanism. These two competitive processes, one for the conventional impurity mechanism and another for the stress-release mechanism, are probably the reasons that contribute to the observed change of grain sizes.

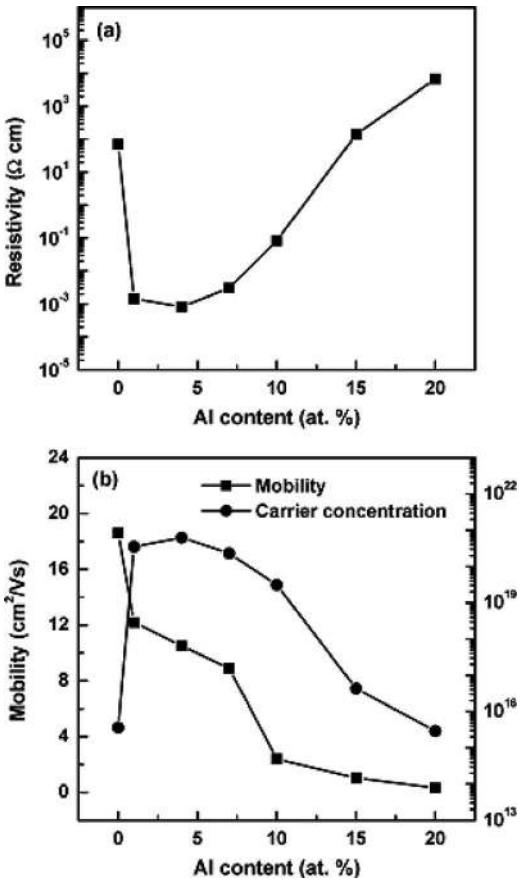

FIG. 10. Carrier concentration, Hall mobility, and resistivity of (Zn,Al)O films as a function of the Al content in the 0–20 at. % range. They are shown in (a) and (b) for convenient illustrations.

E. Electrical properties

The electrical properties were investigated by Hall effect measurements. Figure 10 shows how the electrical resistivity (ρ), Hall mobility (μ_H), and carrier concentration (n_e) of (Zn,Al)O films are related to the Al content ranging from 0 to 20 at. %. At the high Al contents such as 30 and 50 at. %, the film resistivity is too high to be measured by a Hall system, and thus is not included in Fig. 10. To illustrate the electrical properties of the two kinds of films, spreading resistance profiles (SRPs) were performed, showing their resisitivity in the 10^6–10^7 Ω cm range. Figure 10(a) shows the variation of resistivity of (Zn,Al)O films with respect to the Al content. The resistivity is about 70.7 Ω cm for the undoped ZnO film. By introduction of Al in ZnO, the electrical resistivity is greatly reduced. For example, the resistivity is about 1.45×10^{-3} Ω cm at 1 at. % Al, and then decreases to 8.21×10^{-4} Ω cm at 4 at. % Al, which is the minimum value obtained for AZO films, six orders of magnitude lower than that of undoped samples. As the Al content is up to 7 at. %, the film resistivity is 3.03×10^{-3} Ω cm. With further increasing Al content in (Zn,Al)O films, a rapid increase in resistivity appears, from 8.35×10^{-2} Ω cm at 10 at. % Al up to 1.39×10^{2} Ω cm at 15 at. % Al to 6.69×10^{4} Ω cm at 20 at. % Al. This is an indication that, in order to get highly conducting AZO films, it is necessary to deliberately optimize the amount of Al in ZnO. The resistivity of the (Zn,Al)O film is related to the Al-doping concentration, intrinsic defects (e.g., Zn interstitials and O vacancies), respective concentrations of Al atoms at substitutional and interstitial sites, and various scattering centers. The resistivity (ρ) is proportional to the reciprocal of the product of the electron concentration (n_e) and the mobility (μ_H).

The carrier concentrations of (Zn,Al)O films are shown in Fig. 10(b). The electron concentration of undoped ZnO film is about 3.6×10^{15} cm^{-3}, which could be enhanced drastically by the Al incorporation. As the Al content increases from 1 to 7 at. %, the electron concentration first increases and then decreases, reaching a maximum value of 6.2×10^{20} cm^{-3} at 4 at. % Al. It is noted that the electron concentrations are always more than 10^{20} cm^{-3} in the 1–7 at. % doping content range and nearly constant in principle regardless of the amount of Al in the film, implying that these deposited AZO films are degenerate semiconductors. As the Al content is up to 10 at. %, the electron concentration decreases to 3.1×10^{19} cm^{-3}. The above behavior of electron concentration suggests that not all the Al atoms in the film contribute to donor dopants. When a small amount of Al impurities are added to ZnO, they mostly substitute Zn existing at lattice sites as donors, together with less Al atoms present at interstitial sites. This is in the low Al content region (e.g., 1, 4, and 7 at. %), in which a highly conducting AZO film with an optimum Al-doping concentration is obtained. However, when the Al content is above a certain critical concentration and located at 10 at. %, for example, excess Al atoms in the film result in the intragrain congregation and/or grain-boundary segregation forming Al–Al and Al–O clusters such as AlO_x suboxides. These Al atoms are electrically inactive, even acting as "electron killers" with such effects as donor passivation; thus the electron concentrations are limited. Similar suggestions were proposed by Chen *et al.*[20] and Choi *et al.*[32] for ZnO:Al and ZnO:Ga films, respectively. We provide the experimental evidences supporting this suggestion by observing the formation of Al_2O_3 phase in (Zn,Al)O films in this work. As the Al content increases to 15 at. % Al, the electron concentration is reduced to 4.3×10^{16} cm^{-3}, followed by a significant drop to 2.9×10^{15} cm^{-3} at a higher Al content of 20 at. %. The much lower concentrations imply that the element precipitation is evident. This degradation derived from Hall effect results is in good agreement with the XRD and SEM observations. The second-phase separation is observed in the (Zn,Al)O film with a 30 at. % Al content, and accordingly it is highly resistant. Similarly, it is easy to understand the much higher resistivity of the (Zn,Al)O film with a 50 at. % Al content, since its matrix is Al_2O_3.

Figure 10(b) shows the Hall mobility of (Zn,Al)O films. The mobility decreases gradually with the increase in Al content in films from ~18.6 cm^2 V^{-1} s^{-1} for pure ZnO to ~0.32 cm^2 V^{-1} s^{-1} as the amount of Al increases to 20 at. %. The carrier mobility is determined by a few scattering mechanisms. It is necessary to analyze various scattering mechanisms not only to understand the causes of this decrease in mobility but also to provide useful information to improve the mobility by decreasing the number of scattering centers in films. For polycrystalline (Zn,Al)O films, the carrier mobility may be expressed as

$$\frac{1}{\mu_H}=\frac{1}{\mu_i}+\frac{1}{\mu_n}+\frac{1}{\mu_g}+\frac{1}{\mu_c}+\frac{1}{\mu_l}. \tag{6}$$

Here, μ_i, μ_n, μ_g, μ_c, and μ_l are mobilities due to ionized impurity scattering, neutral impurity scattering, grain-boundary scattering, intragrain cluster scattering, and lattice vibration scattering, respectively.

(1) Ionized impurity scattering (μ_i). The ionized impurity scattering mobility is expressed as[12,21]

$$\mu_i=\left(\frac{2}{m_c^*}\right)^{1/2}\frac{\varepsilon^{1/2}E_F^{3/2}}{\pi e^3 N_i Z^2}\left[\ln\left(1+\frac{\varepsilon E_F}{N_i^{1/3}Ze^2}\right)^2\right]^{-1}, \tag{7}$$

where E_F, ε, e, and Z are the Fermi level, static dielectric constant, electron charge, and ion valence, respectively. Also, $m_c^*=0.38m_0$ is the electron effective mass in conduction band. N_i is the concentration of the scattering centers, which can be considered to be approximately equal to the electron concentration (n_e) for the degenerate AZO films (1–7 at. % Al). As compared with pure ZnO ($\sim$18.6 cm^2 V^{-1} s^{-1}), the mobility exhibits an abrupt decrease to $\sim$12.2 cm^2 V^{-1} s^{-1} for the AZO film with a 1 at. % Al content. This change is due to the significantly enhanced concentration of ionized impurity because of the Al incorporation. For highly degenerate semiconductors, the ionized impurity scattering is the main scattering mechanism, independent of temperature in the low temperature region including room temperature. The carrier mobility decreases from 12.2 cm^2 V^{-1} s^{-1} at 1 at. % to 10.5 cm^2 V^{-1} s^{-1} at 4 at. % to 8.9 cm^2 V^{-1} s^{-1} at 7 at. %. This variation is relatively small, exhibiting one of the behaviors of the ionized impurity scattering for degenerate semiconductors. Previous studies by Young *et al.*,[70] Pei *et al.*,[21] and Agashe *et al.*[22] reached the same conclusions with different approaches. The ionized impurity scattering is the dominant scattering mechanism in the range of $N_e>10^{20}$ cm^{-3} for Al-doped ZnO.

(2) Neutral impurity scattering (μ_n). For undoped and Al-doped ZnO films, the amount of neutral impurity scattering centers is much less than that of the ionized impurity. The neutral impurity scattering could be negligible.

(3) Grain-boundary scattering (μ_g). The free-electron mean free path of the carriers in films is calculated using the following formula:[21,71]

$$L=\left(\frac{h}{2e}\right)\left(\frac{3n_e}{\pi}\right)^{1/3}\mu_H, \tag{8}$$

where h is Planck's constant. The calculated value is less than 4.5 nm, which is usually much smaller than the grain size observed in our experiments, so the grain-boundary scattering has little effect on the observed carrier mobility. The grain-boundary scattering is dominant only when its grain sizes are comparable to the mean free path. According to the scattering model of grain boundary, mobility is written as:[12,72]

$$\mu_g=\mu_0 T^{-1/2}\exp(-\Delta E/kT). \tag{9}$$

Here, ΔE is the potential barrier of grain boundary, k is the Boltzmann constant, and T is the temperature. The decrease in grain size enhances the grain-boundary scattering, which possibly plays an important role in determining the carrier translation in (Zn, Al)O films with the Al contents of 30 and 50 at. %, since their grain sizes are very small. In addition, the increment of surface roughness and film looseness with porosity results in the easiness of chemisorption of nitrogen and/or oxygen, leading to the increase of the barrier height, and thus lowers the carrier mobility. In this regard, the grain-boundary scattering probably contributes more to the observed low mobility of the (Zn, Al)O film with a relatively high Al content such as 20 at. %.

(4) Lattice vibration scattering (μ_l). The lattice vibration scattering mobility is given by[21,31]

$$\mu_l=\left(\frac{\pi}{3}\right)^{1/3}\frac{eh^3C_l}{(m_c^*)^2E_d^2kT}\frac{1}{n_e^{1/3}}\propto\frac{1}{T}. \tag{10}$$

Here, C_l is the elasticity modulus and E_d is the deformation potential constant. The lattice vibration scattering is dominant in the high temperature range. Its contribution could be negligible at room temperature.

(5) Intragrain cluster scattering (μ_c). Figure 10(b) exhibits a sharp decrease in carrier mobility from 8.9 cm^2 V^{-1} s^{-1} at 7 at. % Al to 2.4 cm^2 V^{-1} s^{-1} at 10 at. % Al. A similar drastic change was previously reported in the 4–10 at. % Al content region. The reason is still controversial. This change was once ascribed to the grain-boundary scattering,[16,23,73] but further studies questioned its reasonability.[21,71] Our experiments also reveal that the grain-boundary scattering has little effect on the observed mobility at the Al contents lower than 20 at. %. Thus, an acceptable explanation for this abrupt variation was not yet reached. For this purpose, we propose an intragrain cluster scattering mechanism here to interpret the observations. As mentioned above, the heavy incorporation of Al leads to the intragrain congregation forming various clusters such as Al–Al and Al–O. These clusters can affect not only the inclusion of electrically active dopants but also the mobility considering the increase of scattering centers. This behavior is anticipated as the consequence of the heavy incorporation of Al into ZnO films. Although the grain sizes are larger than the electron mean free path, the intragrain cluster scattering probably plays a crucial role in determining the electron translation in these films. This effects need to be seriously considered. Besides the ionized impurity scattering, the intragrain cluster scattering may be another important factor that accounts for the rapid decrease in carrier mobility of AZO films in the 4–10 at. % Al content region.

F. Optical properties

The optical transmission was measured by a UV-Vis spectrophotometer. Figure 11 gives the spectra for all the (Zn, Al)O films. For convenient illustrations, they are displayed in Figs. 11(a) and 11(b). The fluctuation in the spectra is principally due to the interference effect owing to the reflection at interfaces. Sharp fundamental absorption edges are observed in all the spectra corresponding to the (Zn, Al)O films in the 0–10 at. % Al range. These films have a high transmittance (about 90%) in visible regions and a high absorption (near 100%) in UV regions. As the Al content is up

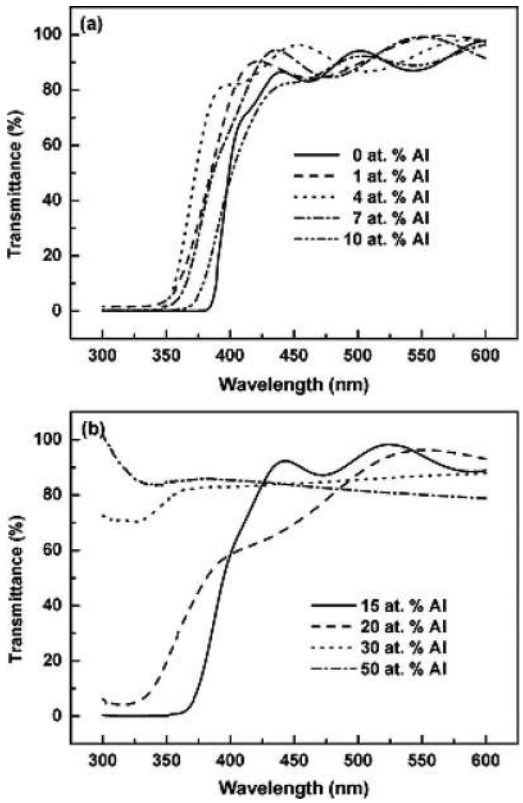

FIG. 11. Optical transmission spectra of (Zn,Al)O films prepared with the Al contents of 0, 1, 4, 7, 10, 15, 20, 30, and 50 at. %. They are shown in (a) and (b) for convenient illustrations.

to 15 and 20 at. %, the fundamental absorption edges become much gentler, with the reduction of the transmittance in visible regions and the absorption in UV regions, which is mainly attributed to the degradation of crystal quality. At a 30 at.% Al content, the (Zn, Al)O film is of two phases, ZnO and Al_2O_3. In the ZnO–MgO two-phase film,[74] the optical transmission with double edges, one for ZnO and another for MgO, was observed. Accordingly, it is reasonable to anticipate similar behaviors in the ZnO–Al_2O_3 two-phase film. The edge that appeared at about 345 nm is attributed to ZnO, and another edge is expected to be located at around 124 nm corresponding to the band gap (9.0 eV) of Al_2O_3, although it could not be observed in our cases due to the limitedly investigated wavelength range. As the Al content is 50 at. %, the transmission of the film exhibits the behavior of Al_2O_3 since the matrix is Al_2O_3, and almost no trace from ZnO is observed except a valley that appeared at ~340 nm probably reflecting its effect.

In the following discussion, we mainly focus on the optical properties of (Zn, Al)O films in the 0–10 at. % Al content range. The fundamental absorption, which corresponds to the electron excitation from valance band to conduction band, is usually used to determine the value of optical band gap (E_g). As a direct band gap semiconductor, ZnO has an absorption coefficient (α) obeying the following relation for high photon energies ($h\nu$):

$$\alpha(h\nu) = C(h\nu - E_g)^{1/2}. \tag{11}$$

Here, C is a constant and ν is the photon frequency. The absorption coefficient (α) is defined as

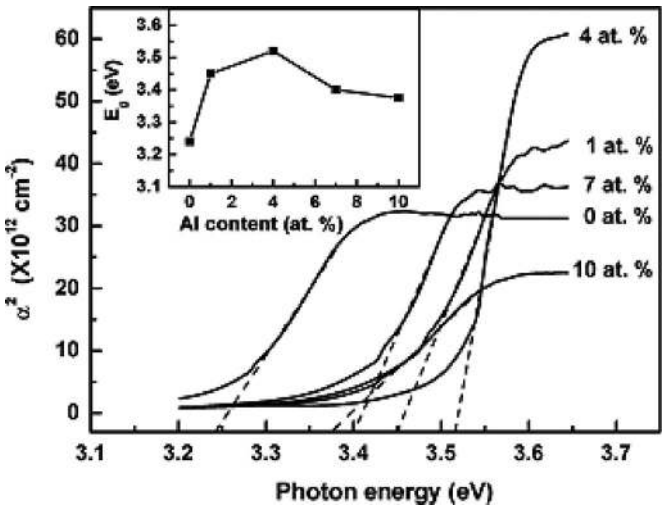

FIG. 12. Plot of square of the absorption coefficient vs photon energy for (Zn,Al)O films prepared with the Al contents of 0, 1, 4, 7, and 10 at. %. The inset shows the optical band-gap energies as a function of the Al content.

$$I = I_0 \exp(-\alpha t), \tag{12}$$

where I and I_0 are the intensities of transmitted and incident light, respectively, and t is the film thickness. Considering interfaces related to the film and the film thickness in practical experiments, the transmittance (T) and reflectivity (R) of the film obey the following relation:[75]

$$T = (1-R)^2 \exp(-\alpha t). \tag{13}$$

Thus, α could be calculated from the above equation; that is,

$$\alpha = -1/t \ln[T/(1-R)^2]. \tag{14}$$

The optical band gap values, such as those shown in Fig. 12, are determined from Eq. (11) by plotting the square of the optical absorption coefficient as a function of the photon energy and by extrapolating the linear region to the energy axis. The thus determined values are shown in the inset of Fig. 12. With increasing Al content from 0 to 10 at. %, the band gap of AZO films first increases, and then decreases, reaching the maximum value of 3.52 eV at 4 at. % Al, which coincides with the highest electron concentration. This movement of the band gap is explained by the cause of the Burstein-Moss (BM) shift,[76] an energy band widening (blueshift) effect resulting from the increase of the Fermi level in the conduction band of degenerate semiconductors. If we assume that the Fermi surface is spherical, the following well-known formula is given:

$$E_g = E_g^0 + \Delta E_g^{\mathrm{BM}}. \tag{15}$$

Here, E_g and E_g^0 are the band gap energies of doped and intrinsic ZnO, respectively. Also, ΔE_g^{BM} is the energy band gap widening (BM shift), which is related to the electron concentration through the following equation:[76,77]

$$\Delta E_g = \frac{h^2}{8m_c^*}\left(\frac{3}{\pi}\right)^{2/3} n_e^{2/3}. \tag{16}$$

Figure 13 shows the correlation between the blueshift of the band gap and the electron concentration. The blueshift of the gap energy is proportional to the electron concentration but

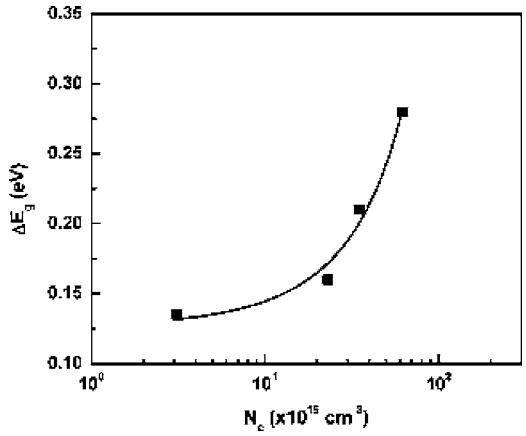

FIG. 13. Dependence of the optical band-gap blueshift on the electron concentration in AZO films.

does not accurately follow Eq. (16). The exponent in Eq. (16) is 2/3, but the experimental value is ~1/2. A similar derivation toward a low value was reported in other experiments,[16,32,77,78] showing that the exponent is in the range of 1/3–2/3. At a high carrier concentration above the Mott critical concentration $\sim 10^{20}$ cm^{-3} in ZnO,[77,79] the electronic states of the material are modified because of the electron-electron and electron-impurity interactions; that is, the many-body effects such as exchange and Coulomb interactions make the band gap narrow.[80,81] This phenomenon is in competition with the BM shift for a semiconductor. Thus, the exponent of n_e obtained from experimental value is not exactly equal to, and always lower than, that in Eq. (16). This is the Burstein-Moss shift with the modulation of many-body effects.

IV. CONCLUSION

In summary, we have prepared (Zn, Al)O thin films by dc reactive magnetron sputtering in a wide range of Al content from 0 to 50 at. %. The (Zn, Al)O films were systematically examined for having a comprehensive knowledge of their behaviors. The growth rate of (Zn, Al)O films is monotonically reduced with increasing Al content. The amount of Al in the film is nearly the same as that in the target, but often with an Al content dependent deviation towards a somewhat lower value as compared with the latter.

(1) In a low Al content region (<10 at. %). The *n*-type AZO thin films could be obtained at 400 °C in an Ar–O_2 ambient with good properties, such as a low resistivity $\sim 10^{-4}$ Ω cm, a high transmittance ~90% in visible regions, and an acceptable crystal quality with a high (002) preferential orientation. The optimum Al content is 4 at. %. This appropriate Al-doping concentration effectively serves to release the residual, compressive stress in the plane of the AZO film, which is believed to be the reason for the improved film stability and the increased grain size. As for the degenerate AZO films with the electron concentration above 10^{20} cm^{-3}, the ionized impurity scattering is the main scattering mechanism. Their band gap energies are evidently widened as compared with intrinsic ZnO (e.g., 3.52 eV at 4 at. % Al), which is due to the Burstein-Moss shift with the modulation of many-body effects.

(2) In a medium Al content region (10–30 at. %). The crystal quality of ZnO:Al thin films is degraded, even with the appearance of additional diffraction peaks such as (100) and (101) besides the (002) plane, but they still exhibit a single-phase wurtzite ZnO structure. The solubility limit of Al in ZnO films is in the 20–30 at. % range, which is much higher than the thermodynamic solubility limit of 2–3 at. % in ZnO at an equilibrium state. The electron concentration is greatly reduced as the consequence of the intragrain congregation and grain-boundary segregation forming clusters such as Al–Al and Al–O. An intragrain cluster scattering mechanism is proposed in this work to explain the much lower carrier mobility of films in this region, with an abrupt decrease from 8.9 cm^2 V^{-1} s^{-1} at 7 at. % Al to 2.4 cm^2 V^{-1} s^{-1} at 10 at. % Al. The ZnO:Al films also exhibit an evident degradation in optical quality, such as the gentle fundamental absorption edges and the reduced transmittance in visible regions.

(3) In a high Al content region (>30 at. %). There is an apparent variation for (Zn, Al)O films. At the Al content of 30 at. %, the film is composed of two phases, ZnO hexagonal and Al_2O_3 rhombohedral structures. The matrix of the (Zn, Al)O film is Al_2O_3 at 50 at. % Al, and no evident trace of wurtzite ZnO is observed. These results are well in agreement with observations from the electrical and optical measurements.

ACKNOWLEDGMENTS

This work was supported by the Key Project of National Natural Science Foundation of China under Grant No. 50532060, National Natural Science Foundation of China under Grant No. 50572095, and National Postdoctoral Foundation of China under Grant No. 2005038620.

[1] Z. K. Tang, G. K. L. Wong, P. Yu, M. Kawasaki, A. Ohtomo, H. Koinuma, and Y. Segawa, Appl. Phys. Lett. **72**, 3270 (1998).
[2] D. C. Look, D. C. Reynolds, J. R. Sizelove, R. L. Jones, C. W. Litton, G. Cantwell, and W. C. Harsch, Solid State Commun. **105**, 399 (1998).
[3] D. M. Bagnall, Y. F. Chen, Z. Zhu, T. Yao, S. Koyama, M. Y. Shen, and T. Goto, Appl. Phys. Lett. **70**, 2230 (1997).
[4] A. Ohtomo *et al.*, Appl. Phys. Lett. **72**, 2466 (1998).
[5] K. Koike, K. Hama, I. Nakashima, G. Takada, K. Ogata, S. Sasa, M. Inoue, and M. Yano, J. Cryst. Growth **278**, 288 (2005).
[6] T. Makino, Y. Segawa, M. Kawasaki, A. Ohtomo, R. Shiroki, K. Tamura, T. Yasuda, and H. Koinuma, Appl. Phys. Lett. **78**, 1237 (2001).
[7] Z. Z. Ye, D. W. Ma, J. H. He, J. Y. Huang, B. H. Zhao, X. D. Luo, and Z. Y. Xu, J. Cryst. Growth **256**, 78 (2003).
[8] G. Xiong, J. Wilkinson, B. Mischuck, S. Tüzemen, K. B. Ucer, and R. T. Williams, Appl. Phys. Lett. **80**, 1195 (2002).
[9] V. Gupta and A. Mansingh, J. Appl. Phys. **80**, 1063 (1996).
[10] W. W. Wenas, A. Yamada, K. Takahashi, M. Yoshino, and M. Konagai, J. Appl. Phys. **70**, 7119 (1991).
[11] B. J. Lokhande, P. S. Patil, and M. D. Uplane, Physica B **302/303**, 59 (2001).
[12] J. Ma, F. Ji, D. H. Zhang, H. L. Ma, and S. Y. Li, Thin Solid Films **357**, 98 (1999).
[13] K. Ellmer and R. Wendt, Surf. Coat. Technol. **93**, 21 (1997).
[14] K. Ellmer, F. Kudella, R. Mientus, R. Schieck, and S. Fiechter, Thin Solid Films **247**, 15 (1994).
[15] Y. Igasaki and H. Saito, J. Appl. Phys. **70**, 3613 (1991).
[16] K. H. Kim, K. C. Park, and D. Y. Ma, J. Appl. Phys. **81**, 7764 (1997).
[17] R. Cebulla, R. Wendt, and K. Ellmer, J. Appl. Phys. **83**, 1087 (1998).

[18]D. J. Cohen, K. C. Ruthe, and S. A. Barnett, J. Appl. Phys. **96**, 459 (2004).
[19]S. S. Lin, J. L. Huang, and P. Šajgalik, Surf. Coat. Technol. **185**, 254 (2004).
[20]M. Chen, X. Wang, Y. H. Yu, Z. L. Pei, X. D. Bai, C. Sun, R. F. Huang, and L. S. Wen, Appl. Surf. Sci. **158**, 134 (2000).
[21]Z. L. Pei, C. Sun, M. H. Tan, J. Q. Xiao, D. H. Guan, R. F. Huang, and L. S. Wen, J. Appl. Phys. **90**, 3432 (2001).
[22]C. Agashe, O. Kluth, J. Hüpkes, U. Zastrow, B. Rech, and M. Wuttig, J. Appl. Phys. **95**, 1911 (2004).
[23]G. Fang, D. Li, and B. Yao, Vacuum **68**, 363 (2003).
[24]A. Martín, J. P. Espinós, A. Justo, J. P. Holgado, F. Yubero, and A. R. González-Elipe, Surf. Coat. Technol. **151/152**, 289 (2002).
[25]J. Mass, P. Bhattacharya, and R. S. Katiyar, Mater. Sci. Eng., B **B103**, 9 (2003).
[26]H. Kim *et al.*, Appl. Phys. Lett. **76**, 259 (2000).
[27]M. Kumar, R. M. Mehra, A. Wakahara, M. Ishida, and A. Yoshida, J. Appl. Phys. **93**, 3837 (2003).
[28]T. Makino, K. Tamura, C. H. Chia, Y. Segawa, M. Kawasaki, A. Ohtomo, and H. Koinuma, Phys. Status Solidi B **229**, 853 (2002).
[29]A. E. Jiménez-González, J. A. S. Urueta, and R. Suárez-Parra, J. Cryst. Growth **192**, 430 (1998).
[30]P. Nunes, E. Fortunato, P. Tonello, F. B. Fernandes, P. Vilarinho, and R. Martins, Vacuum **64**, 281 (2002).
[31]M. N. Islam, T. B. Ghosh, K. L. Chopra, and H. N. Acharya, Thin Solid Films **280**, 20 (1996).
[32]B. H. Choi, H. B. Im, J. S. Song, and K. H. Yoon, Thin Solid Films **193/194**, 712 (1990).
[33]H. J. Ko, Y. F. Chen, S. K. Hong, H. Wenisch, T. Yao, and D. C. Look, Appl. Phys. Lett. **77**, 3761 (2000).
[34]T. Makino, Y. Segawa, S. Yoshida, A. Tsukazaki, A. Ohtomo, and M. Kawasaki, Appl. Phys. Lett. **85**, 759 (2004).
[35]M. Miki-Yoshida, F. Paraguay-Delgado, W. Estrada-López, and E. Andrade, Thin Solid Films **376**, 99 (2000).
[36]Th. Agne, Z. Guan, X. M. Li, H. Wolf, Th. Wichert, H. Natter, and R. Hempelmann, Appl. Phys. Lett. **83**, 1204 (2003).
[37]T. Minami, T. Yamamoto, and T. Miyata, Thin Solid Films **366**, 63 (2000).
[38]T. Minami, H. Sato, H. Nanto, and S. Takata, Jpn. J. Appl. Phys., Part 2 **25**, L776 (1986).
[39]R. P. Wang, L. L. H. King, and A. W. Sleight, J. Mater. Res. **11**, 1659 (1996).
[40]B. M. Ataev, A. M. Bagamadova, V. V. Mamedov, A. K. Omaev, and M. R. Rabadanov, J. Cryst. Growth **198/199**, 1222 (1999).
[41]H. Y. Xu, Y. C. Liu, R. Mu, C. L. Shao, Y. M. Lu, D. Z. Shen, and X. W. Fan, Appl. Phys. Lett. **86**, 123107 (2005).
[42]J.-M. Ntep, S. Said Hassani, A. Lusson, A. Tromson-Carli, D. Ballutaud, G. Didier, and R. Triboulet, J. Cryst. Growth **207**, 30 (1999).
[43]S. Takata, T. Minami, and H. Nanto, Thin Solid Films **135**, 183 (1986).
[44]D. S. Ginley and C. Bright, MRS Bull. **25**, 15 (2000).
[45]H. Kim, J. S. Horwitz, G. P. Kushto, Z. H. Kafafi, and D. B. Chrisey, Appl. Phys. Lett. **79**, 284 (2001).
[46]D. Song, A. G. Aberle, and J. Xia, Appl. Surf. Sci. **195**, 291 (2002).
[47]D. C. Look and B. Claflin, Phys. Status Solidi B **241**, 624 (2004).
[48]J. G. Lu, Z. Z. Ye, L. Wang, B. H. Zhao, and J. Y. Huang, Chin. Phys. Lett. **19**, 1494 (2002).
[49]J. G. Lu, Y. Z. Zhang, Z. Z. Ye, L. Wang, B. H. Zhao, and J. Y. Huang, Mater. Lett. **57**, 3311 (2003).
[50]J. G. Lu, Z. Z. Ye, F. Zhuge, Y. J. Zeng, B. H. Zhao, and L. P. Zhu, Appl. Phys. Lett. **85**, 3134 (2004).
[51]Y. R. Ryu, W. J. Kim, and H. W. White, J. Cryst. Growth **219**, 419 (2000).
[52]F. Zhuge *et al.*, Appl. Phys. Lett. **87**, 092103 (2005).
[53]J. G. Lu, L. P. Zhu, Z. Z. Ye, F. Zhuge, B. H. Zhao, L. Wang, J. Y. Huang, and J. Yuan, J. Cryst. Growth **283**, 413 (2005).
[54]H. K. Kim, K. K. Kim, S. J. Park, T. Y. Seong, and I. Adesida, J. Appl. Phys. **94**, 4225 (2003).
[55]H. K. Kim, T. Y. Seong, K. K. Kim, S. J. Park, Y. S. Yoon, and I. Adesida, Jpn. J. Appl. Phys., Part 1 **43**, 976 (2004).
[56]G. D. Yuan, Z. Z. Ye, L. P. Zhu, J. Y. Huang, Q. Qian, and B. H. Zhao, J. Cryst. Growth **268**, 169 (2004).
[57]W. S. Hong, L. C. De Jonghe, X. Yang, and M. N. Rahaman, J. Am. Ceram. Soc. **78**, 3217 (1995).
[58]S. K. Sampath and J. F. Cordaro, J. Am. Ceram. Soc. **81**, 649 (1998).
[59]C. R. Gorla, W. E. Mayo, S. Liang, and Y. Lu, J. Appl. Phys. **87**, 3736 (2000).
[60]M. H. Yoon, S. H. Lee, H. L. Park, H. K. Kim, and M. S. Jang, J. Mater. Sci. Lett. **21**, 1703 (2002).
[61]S. Maniv, W. D. Westwood, and E. Colombini, J. Vac. Sci. Technol. **20**, 162 (1982).
[62]J. G. Lu, Z. Z. Ye, J. Y. Huang, B. H. Zhao, and L. Wang, Chin. J. Semicond. **24**, 729 (2003).
[63]T. Hanabusa, H. Hosoda, K. Kusaka, and K. Tominaga, Thin Solid Films **343/344**, 164 (1999).
[64]P. Nunes, A. Malika, B. Fernandesa, E. Fortunato, P. Vilarinho, and R. Martins, Vacuum **52**, 45 (1999).
[65]S. A. Studenikin, N. Golego, and M. Cocivera, J. Appl. Phys. **87**, 2413 (2000).
[66]M. Copel, M. C. Reuter, E. Kaxiras, and R. M. Tromp, Phys. Rev. Lett. **63**, 632 (1989).
[67]N. Grandjean, J. Massies, and V. H. Etgens, Phys. Rev. Lett. **69**, 796 (1992).
[68]M. Copel, M. C. Reuter, M. H. von Hoegen, and R. M. Tromp, Phys. Rev. B **42**, 11682 (1990).
[69]D. J. Eaglesham, F. C. Unterwald, and D. C. Jacobson, Phys. Rev. Lett. **70**, 966 (1993).
[70]D. L. Young, T. J. Coutts, V. I. Kaydanov, A. S. Gilmore, and W. P. Mulligan, J. Vac. Sci. Technol. A **18**, 2978 (2000).
[71]M. Chen, Z. L. Pei, X. Wang, Y. H. Yu, X. H. Liu, C. Sun, and L. S. Wen, J. Phys. D **33**, 2538 (2000).
[72]T. Minami, H. Nanto, S. Shooji, and S. Takata, Thin Solid Films **111**, 167 (1984).
[73]S. Ghosh, A. Sarkar, S. Chaudhuri, and A. K. Pal, Thin Solid Films **205**, 64 (1991).
[74]I. Takeuchi, W. Yang, K. S. Chang, M. A. Aronova, T. Venkatesan, R. D. Vispute, and L. A. Bendersky, J. Appl. Phys. **94**, 7336 (2003).
[75]J. I. Pankove, *Optical Processes in Semiconductors* (Prentice-Hall, Englewood Clifts, NJ, 1971).
[76]E. Burstein, Phys. Rev. **93**, 632 (1954).
[77]A. P. Roth, J. B. Webb, and D. F. Williams, Phys. Rev. B **25**, 7826 (1982).
[78]B. E. Selnelius, K. F. Berggren, Z. C. Zin, I. Hamberg, and C. G. Granqvist, Phys. Rev. B **37**, 10244 (1998).
[79]A. P. Roth, J. B. Webb, and D. F. Williams, Solid State Commun. **39**, 1269 (1981).
[80]P. A. Wolff, Phys. Rev. **126**, 405 (1962).
[81]K. F. Berggren and B. E. Sernelius, Phys. Rev. B **24**, 1971 (1981).
[82]1996 JCPDS—International Centre for Diffraction Data No. 36-1451.
[83]1996 JCPDS—International Centre for Diffraction Data No. 11-0661.